Naser Mehrabi[1]
Systems Design Engineering,
University of Waterloo,
Waterloo, ON N2L 3G1, Canada
e-mail: nmehrabi@uwaterloo.ca

Reza Sharif Razavian
Systems Design Engineering,
University of Waterloo,
Waterloo, ON N2L 3G1, Canada
e-mail: rsharifr@uwaterloo.ca

John McPhee
Professor
Fellow ASME
Department of Systems Design Engineering,
University of Waterloo,
Waterloo, ON N2L 3G1, Canada
e-mail: mcphee@uwaterloo.ca

A Physics-Based Musculoskeletal Driver Model to Study Steering Tasks

Realistic driver models can play an important role in developing new driver assistance technologies. A realistic driver model can reduce the time-consuming trial-and-error process of designing and testing products, and thereby reduce the vehicle's development time and cost. A realistic model should provide both driver path planning and arm motions that are physiologically possible. The interaction forces between a driver's hand and steering wheel can influence control performance and steering feel. The aim of this work is to develop a comprehensive yet practical model of the driver and vehicle. Consequently, a neuromuscular driver model in conjunction with a high-fidelity vehicle model is developed to learn and understand more about the driver's performance and preferences, and their effect on vehicle control and stability. This driver model can provide insights into task performance and energy consumption of the driver, including fatigue and cocontraction dynamics of a steering task. In addition, this driver model in conjunction with a high-fidelity steering model can be used to develop new steering technologies such as electric power steering. [DOI: 10.1115/1.4027333]

1 Introduction

The steering system is the major part of a vehicle with which the driver interacts. For better comfort and stability, many assistive systems (e.g., electric power steering, (EPS)) have been developed. These technologies aim to aid the driver in performing driving tasks, and to improve the *steering feel*.

To better design a steering system, the driver's characteristics (including strength and response time) must be considered; developing driver-based technologies requires proper understanding of the driver. Unfortunately, our understanding of a driver's behavior is still insufficient, especially in interaction with the steering system. The goal of this paper is to present a physics-based simulation framework for further study of driver/vehicle interactions—a tool that can expedite the development process of steering systems by eliminating the need for trial-and-error iterations.

So far, the majority of research on human steering systems has considered a path-following driver model [1–4]. In such models, the physiological characteristics and limitations of the driver are usually neglected. A minority of research papers have followed a different approach and focused on the human neuromuscular system, which gives insight into task performance, disturbance rejection, and energy consumption [5–9]. For example, Pick and Cole in a series of papers [9–12] introduced a neuromuscular system model of the driver with a linear representation of arm dynamics, and studied the effect of steering torque feedback as well as muscle cocontraction on intrinsic muscle stiffness.

In this research, a physiological three-dimensional musculoskeletal arm model is developed to simulate the driver's arm rotating the steering wheel. The use of such a high-fidelity neuromusculoskeletal model of driver is an advancement in the field of predictive steering systems analysis. This physiological model can include the effects of cocontraction, fatigue, or metabolic energy consumption of a real muscle, and therefore provide more realistic results.

A model predictive controller (MPC) is coupled to this model, which is used as the path-following controller (to represent the vision-based decision making of the brain) [4,13]. The output of the MPC, the prediction of the desired steering wheel angle, is then used to find the corresponding joint torques in the driver's arm, and later to identify the muscle forces required for the maneuver. Furthermore, neural feedback, e.g., the stretch reflex, is included in the driver model for each muscle to enhance our understanding of disturbance rejection and precision control in human limbs. Even though individual parts of this control hierarchy have been introduced in the literature, an integration had not been done in the context of automobile driver modeling.

Using this musculoskeletal framework, we can predict muscle loads, which can be used to quantify objective criteria such as fatigue and muscle cocontraction for drivers of different age, gender, and physical ability, thereby supporting the development of new steering technologies such as EPS and lane-keeping.

2 Dynamical Modeling

To obtain reliable results, both the driver and the vehicle should be accurately modeled. Modeling error in each part will affect the behavior of the other, and interpretation of the data will be obscured. In the following sections, the driver and the vehicle models are presented.

2.1 3D Arm Model. Even though the simplified neuromuscular models used in previous works [9,14] can provide useful insight into dynamical behavior of a muscle activated arm, the range of motion is essentially limited. Therefore, for higher fidelity, and to study broader ranges of steering wheel rotation, we have employed a three-dimensional arm model that opens a new window to the steering task analysis.

Figure 1 shows the schematic of the developed arm. The number of degrees of freedom in this model is smaller than the actual degrees of freedom in a human arm. Unlike the human arm, this model does not allow supination/pronation of the forearm, nor does it allow the internal/external rotation of the shoulder. However, the wrist can rotate about the forearm axis. These degrees of freedom have negligible effect on the kinematics of the steering act for the range of steering angle (± 40 deg) considered here; moreover, the associated muscles (supinator, pronator teres, and subscapularis) have negligible activation during steering [15].

[1]Corresponding author.

Manuscript received November 26, 2013; final manuscript received March 28, 2014; published online January 12, 2015. Assoc. Editor: Parviz Nikravesh.

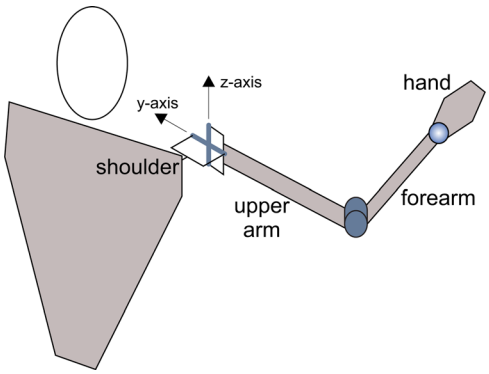

Fig. 1 Schematic view of the 3D arm

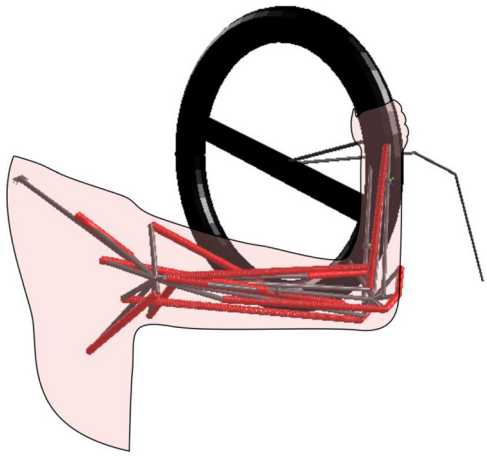

Fig. 2 The muscle-actuated arm model with 14 muscles in MapleSim

Such simplifications reduce the complexity of the model, while maintaining the versatility of the model.

In this 3D arm model, the shoulder and the elbow joints are modeled, respectively, as a universal joint and a revolute joint. The wrist joint is modeled as a spherical joint, and the hand is assumed to be fixed to the steering wheel.

As can be seen in Fig. 1, the arm model consists of four links: the torso, the upper arm (humerus), the forearm (ulna and radius), and the hand. The universal joint connects the humerus to the torso, while the revolute joint attaches the ulna and radius to the humerus. Since the supination or pronation is neglected in this model, the twisting of ulna and radius is not modeled. As a result, the two bones form a rigid structure. The unactuated spherical joint at the wrist connects the hand to ulna/radius. Finally, the hand is firmly attached to the steering wheel, to reduce the complexity. The arm/steering wheel model is, therefore, a one-degree-of-freedom (DoF) mechanism, and the steering wheel angle will fully define all the joint angles.

In total, 14 muscles are used in this model to move the arm (see Fig. 2). The rest of the muscles that are removed are either negligible in effect, or related to the removed degrees of freedom (e.g., supination). Moreover, in spite of significant activity of some wrist actuator muscles during steering [15], the wrist joint is left unactuated because the elbow and shoulder muscles are of the most interest in the steering tasks. Additionally, considering the wrist muscles increases the dimension of the control space, and consequently increases the required computational time to find the optimal muscle forces. Therefore, to speed up the optimization processes, and to run the simulations in a manageable time, the wrist muscles are neglected. The muscle parameters used in this work are taken from Refs. [15,16], and are summarized in Table 1. The muscle origin/insertion coordinates in Table 1 are given with respect to the proximal joint of the related bone. The dimensions and mass and inertia properties of the arm segments are also adopted from Ref. [15], and are summarized in Table 2.

It should be noted that only the right arm is considered in this model. In steering with two hands, drivers tend to steer by pulling the steering wheel downward switching to left and right hands according to the steering direction, while in steering with one hand, both pushing and pulling strategies are employed. Although the two-arm steering is a more realistic condition, we have only modeled one arm for the sake of comparability to other studies [17,18].

The model is prepared in MapleSim, which allows extensive analytical manipulation of equations of motion. Such analytical processing results in highly optimized simulation code.

2.2 Vehicle Dynamics. The vehicle is equally important as the driver, and should be modeled accurately to ensure realistic results. The vehicle model is developed in MapleSim, Fig. 3, and employs a double-wishbone suspension in the front and semitrailing arm in the rear. A rack-and-pinion mechanism is used for the steering, and lastly, a Fiala tire model is used to simulate the road/tire interaction. Full details of the vehicle model are provided in Ref. [19].

3 Driver Model

The driver model in this work is presented as a framework for musculoskeletal analysis of human/vehicle interactions. In humans, the arm motion is controlled by complex commands coming from the central nervous system (CNS). The motor control of humans, and in general that of vertebrates, occurs in a distributed network—all parts of the CNS, including the brain cortex, the cerebellum, and the neural circuits of the spinal cord take part in modulating the motor commands. To study the interactions of the musculoskeletal driver model with the vehicle, the complexity of the motor control network has to be considered. The schematic of a representative motor control hierarchy is shown in Fig. 4. In this model, the control structure consists of two different layers.

The first layer, the supervisory part, is in the form of a feed-forward/feed-back control scheme. This part estimates the required muscle forces based on the states of the system and a prediction of the future path of the vehicle, and is represented as an MPC. The MPC decides on the optimal steering wheel angle based on the current state of the system, vehicle dynamics, and a short-horizon prediction of the future vehicle path. The cost function that the controller tries to minimize is according to the equation below:

$$\theta_{\mathrm{sw}}^{\mathrm{opt}}(k) = \arg\min\left\{\sum_{i=1}^{n_p} q(y(i) - y_{\mathrm{des}}(i))^2 + \sum_{i=1}^{n_c} r(\theta_{\mathrm{sw}}(i))^2\right\} \quad (1)$$

In the above equation, n_p and n_c are the number of prediction and control horizon intervals, respectively; θ_{sw} is the steering wheel angle; and y and y_{des} are the vehicle's lateral position and its desired value, respectively. Lastly, q and r are weighting factors in the cost function.

In our implementation of MPC, the time is discretized into 10 ms intervals, within which the control inputs (the steering wheel angle) are assumed to be constant. The MPC solves the control-oriented model for a number of intervals (called the prediction horizon length) with a certain sequence of control inputs. A linear bicycle model of the vehicle [4] (details in Appendix B) is selected as the control-oriented model to capture the significant dynamics of the vehicle lateral motion. An optimization process then tries to find a sequence that results in the optimal behavior of the system. Once such a control input sequence is found, MPC selects the initial elements of the sequence and applies it to the real system (called the control horizon length). In our path

Table 1 List of muscles included in the 3D arm model

Muscle	Maximum Force (N)	First connection (Origin)	Coordinate (mm)			Second connection (Insertion)	Coordinates (mm)		
			x	y	z		x	y	z
Coracobrachialis (CORB)	120	Torso	20	30	35	Humerus	174	20	0
Deltoid (DELT)	240	Torso	−30	40	15	Humerus	106	−24	−11
Latissimus dorsi (LAT)	360	Torso	−35	90	−125	Humerus	0	0	−13
Pectoralis major (PECM)	210	Torso	45	95	−125	Humerus	17	−13	0
Supraspinatus (SUPSP)	98	Torso	−20	90	35	Humerus	−14	17	27
Infraspinatus (INFRA)	98	Torso	−15	80	−40	Humerus	28	−19	27
Trapezius (TRA)	210	Torso	0	80	10	Humerus	31	0	24
Biceps brachii (BICshort)	100	Torso	0	−15	10	Humerus	252	21	0
Biceps brachii (BIClong)	90	Torso	0	−15	10	Ulna	38	0	10
Triceps brachii (TRIlong)	135	Torso	−25	20	−20	Radius	38	27	−20
Triceps brachii (TRImed)	108	Humerus	78	11	−10	Ulna	38	−27	−15
Anconeus (ANC)	40	Humerus	265	5	−19	Ulna	42	−12	−29
Brachialis (BRA)	167	Humerus	176	−8	16	Radius	33	5	10
Brachioradialis (BRD)	45	Humerus	246	−27	0	Radius	283	−12	0

Table 2 The mass and inertia properties of 3D arm segments

Segment	Mass (kg)	Inertia	$(I_{xx}\ I_{yy}\ I_{zz})$	(g mm^2)[a]	Length (mm)	CoM from proximal (mm)
Humerus	0.945	[0.189	1.46	1.46]	280	140
Ulna	0.376	[0.03	0.417	0.417]	240	78
Radius	0.244	[0.054	0.312	0.312]	240	159
Hand	0.405	[0.220	0.377	0.377]	30	0

[a]Around center of mass, the mechanical x-axis is assumed to be along the bone.

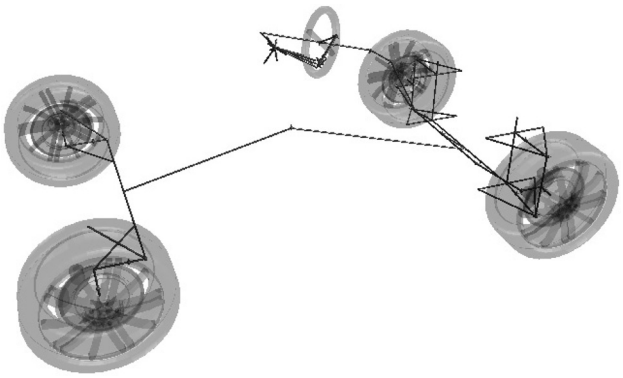

Fig. 3 Vehicle and driver model in MapleSim

following MPC, the prediction horizon length is 250 intervals (2.5 s) and the control horizon length is only two intervals (0.02 s). The choice of the control and prediction horizons is a trade-off between the stability, optimality, and computational time. The influence of control and prediction horizon lengths as well as cost function on the vehicle actual path is fully investigated in Ref. [4].

The output of the MPC controller, the steering wheel angle, is then used to calculate the elbow and shoulder joint torques, which leads to calculation of muscle forces. The details of this procedure will be discussed in Sec. 4.

The second layer of our control hierarchy, the corrective part, provides better control precision and disturbance rejection by means of a feedback control scheme. In human anatomy, the γ-motoneuron activity and stretch reflex are thought to be important mechanisms in improving motion accuracy and attenuating unwanted motions [20,21]. A disturbance or inaccuracy in the limb position is translated into a deviation of the muscle fascicle length from the desired length [22]. The muscle spindle activity, a nonlinear sum of the muscle length and muscle velocity, changes in accordance with the change in fascicle length. The increase or decrease in the afferent signal from the muscle spindle affects the alpha motoneuron activity, which in turn, increases or decreases the muscle force.

In our model, the stretch reflex is modeled as a proportional-derivative (PD) controller. The input to the PD controller is the deviation of the muscle length from its desired value, which is determined by the MPC. Its output represents the afferent signal of the muscle spindle and is added to the reference muscle force to form a monosynaptic stretch reflex mechanism (see Fig. 5). The PD controller parameters are the same for all muscles, and are found by trial-and-error (see Table 3).

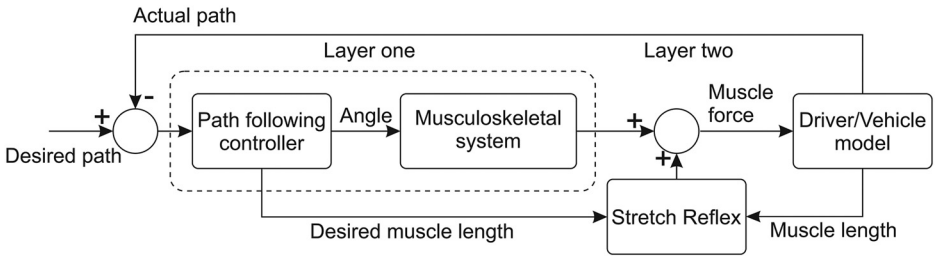

Fig. 4 Workflow of the driver/vehicle model

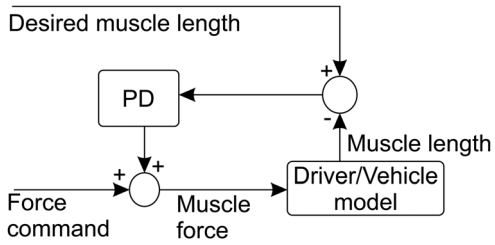

Fig. 5 The PD controller realization of the stretch reflex in the arm model

4 Simulation Procedure

The output of the MPC is the steering wheel angle. Since the driver/steering wheel model is a one-DoF system, the steering wheel angle is enough to solve for all joint angles. To find the optimal joint torques, a simplified model of the vehicle and driver is used. It is argued in Ref. [23] that the nonlinear dynamics of the vehicle can be learned and stored as a set of internal linearized models in the cerebellum. Similarly, we have considered a linear internal model in which the resistive steering torque is modeled by a passive rotational spring and damper. The stiffness K_{sw} and damping coefficient C_{sw} in Eq. (2) have been chosen in a way that the steering dynamics are as close as possible to the high-fidelity vehicle model in the limited speed range of interest.

$$T_{sw} = K_{sw}\theta_{sw} + C_{sw}\dot{\theta}_{sw} \tag{2}$$

Knowing the resistive steering wheel torque and the desired joint motion, the joint torques that generate a similar motion in a forward dynamic setting can be found. Unfortunately, the calculation of such joint torques is not a trivial problem. The system has only one degree of freedom, and three actuators—joint torques at the shoulder and the elbow. This system is an indeterminate dynamic system because the number of actuators is more than the degrees of freedom, which requires an extra criterion to reach a unique solution. Usually this actuator redundancy is solved by assuming that a human minimizes a physiological cost to perform the desired motion [24,25]. Here, an objective function given by Eq. (3) is used in the minimization.

$$T_i^{opt}(k) = \arg\min\left\{w_1\left(\theta_{sw}(k) - \theta_{sw}^{des}(k)\right)^2 + w_2 J_i^2\right\} \tag{3}$$

where w_1 and w_2 are weighting factors in the objective function θ_{sw}^{des} is the desired steering wheel angle from the path-following controller, and θ_{sw} is the actual angle of steering wheel. To find the joint torques and reaction forces, an index of reducing actuator effort is used as the physiological cost function (J_i). As an index of reducing actuator effort, one option is to minimize reaction forces in the wrist joint.

$$J_{reaction} = (R_x)^2 + (R_y)^2 + (R_z)^2 \tag{4}$$

Alternatively, the joint torques can be used in the objective function.

$$J_{torque} = (T_{elbow})^2 + (T_{shoulder-z})^2 + (T_{shoulder-y})^2 \tag{5}$$

In the above relations, R_i is the wrist joint reaction force component and T_i is the joint torque. The optimization problems stated above can be solved using the sequential quadratic programming optimization routines in MATLAB. This gradient-based optimization method tries to minimize the tracking error between desired and actual steering wheel angle, while keeping the objective function, Eqs. (4) or (5), minimized.

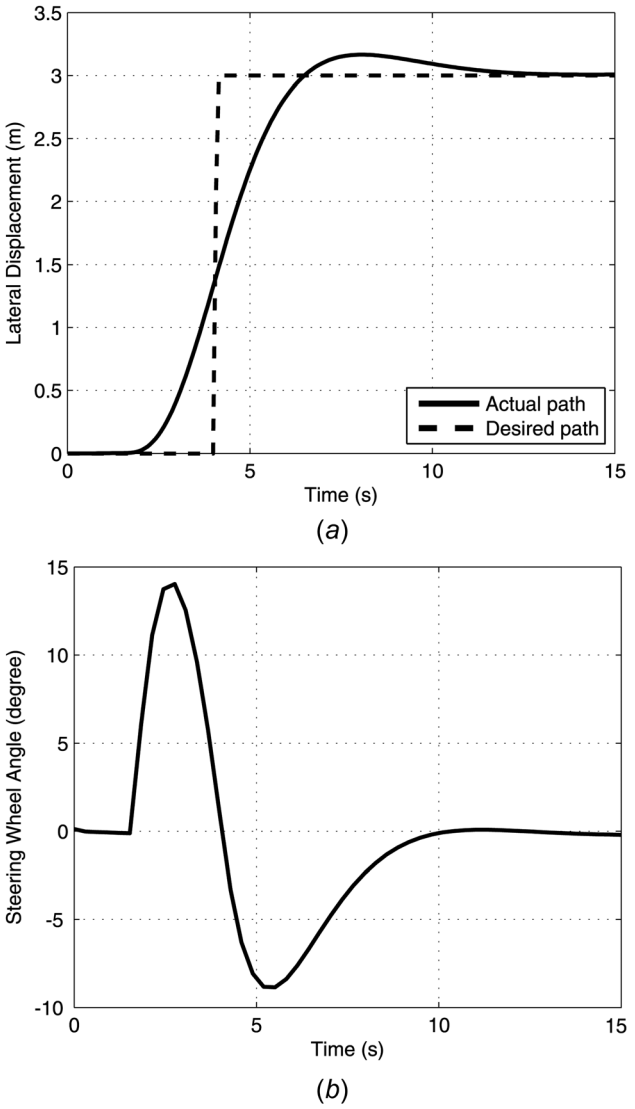

Fig. 6 (*a*) Vehicle lateral position, (*b*) steering wheel angle from path-following controller

The last step in the simulation procedure is the calculation of optimal muscle forces from the joint torques. This can be done by balancing the moments ($\boldsymbol{m}_1$ and $\boldsymbol{m}_2$ in Eq. (6)) at the joints for the torque- and force-actuated systems. Therefore, the relation between the three joint torques and the 14 muscle forces can be found

$$\begin{aligned} &\boldsymbol{m_1}(\boldsymbol{F},\boldsymbol{\theta}) = \boldsymbol{m_2}(\boldsymbol{T},\boldsymbol{\theta}) \qquad \text{or} \\ &\boldsymbol{G}(\boldsymbol{F},\boldsymbol{T},\boldsymbol{\theta}) = \boldsymbol{0} \end{aligned} \tag{6}$$

where $\boldsymbol{G}$ (a 3×1 set of functions) relates the 14 muscle forces to the three joint torques at any given limb position, $\boldsymbol{\theta}$. Therefore the problem of force sharing in this arm has to be solved with a number of assumptions, and in an optimal manner. There are different ways to set up the optimization problem. One of these well-known hypotheses suggests that the CNS minimizes a physiological cost for a given task [26–28]. This cost function can be written as a polynomial function

$$J_{force} = \sum_{i=1}^{14}\left(\frac{f_i}{N_i}\right)^p \tag{7}$$

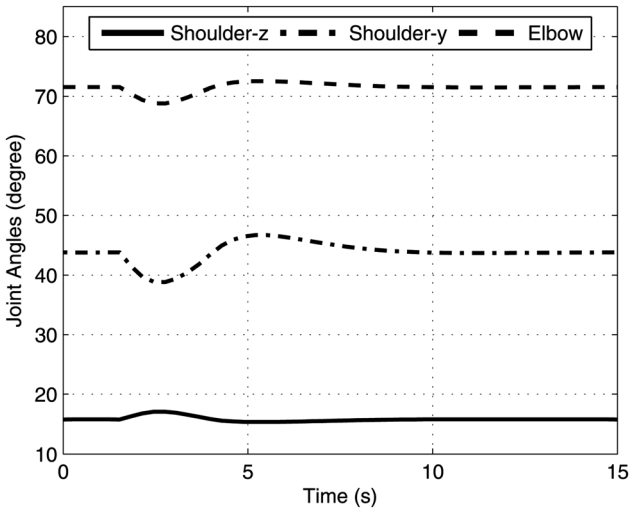

Fig. 7 3D arm joint angles

where f_i is the muscle force, p is the polynomial degree, and N_i is a normalization factor or function. Here, p is assumed to be two, and N_i is chosen to be the maximum isometric force that muscle i can produce.

The cost function is minimized at each time step, using the static optimization procedure, and is subjected to the following inequality constraints:

$$0 \leq F_i \leq F_i^{\max} \tag{8}$$

and equality constraints of Eq. (6) (the values of $\boldsymbol{T}$ and $\boldsymbol{\theta}$ are known at each time step). $F_i^{\max}$ is the maximum isometric muscle force given in Table 1.

An optimization algorithm can be used to solve for the optimal muscle forces. The same optimization routine as the torque distribution optimization has been used to find the optimal muscle forces. The computed muscle forces are then used in the forward dynamic simulation of the muscle actuated driver-vehicle system.

The reflex loop is meant to reduce the effect of disturbances in the system. In this simulation, however, no explicit disturbance is defined. Thus, the stretch reflex loop only

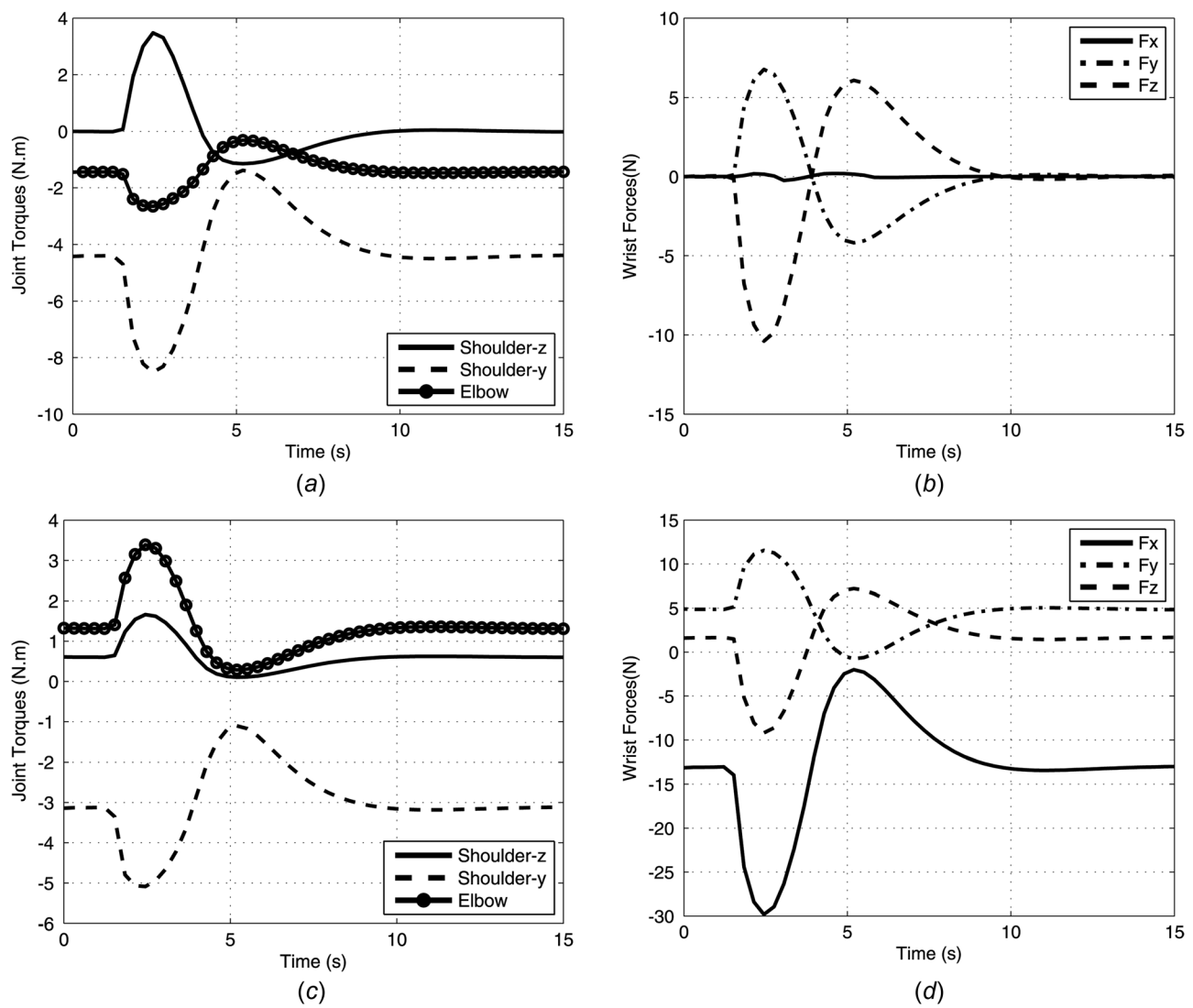

Fig. 8 Joint torques (left) and wrist reaction forces (right) during the lane change maneuver; ((*a*) and (*b*)) with wrist reaction force minimization criterion; ((*c*) and (*d*)) with joint torque minimization criterion. The wrist reaction forces are shown in axial (Fx), radial (Fy), and tangential (Fz) directions of the steering wheel.

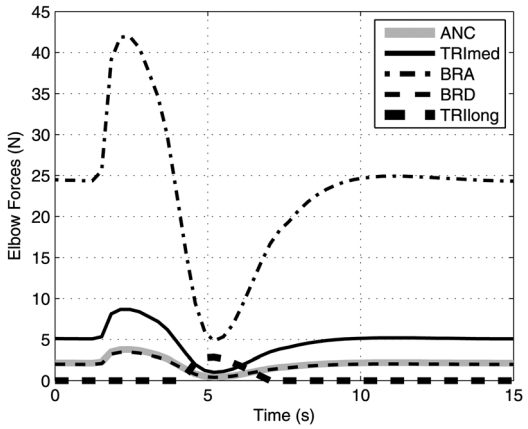

Fig. 9 Optimal muscle forces for the elbow muscles

accounts for the differences between the high-fidelity and the driver's internal models of the arm and vehicle. Additionally, the stretch reflex mechanism is used to compensate for numerical errors due to forward integration, and ensures that the system follows the reference motion. However, in future work, the stretch reflex will be of significance in the study of human/steering interfaces [29]. Unexpected road/tire interactions, such as road irregularities, exert disturbances on the system. Moreover, assistive devices such as EPS and lane-keeping will add torque and angle overlay inputs to the steering system, which excite the human reflex loops.

5 Simulation Results

All simulations are done in the MATLAB/SIMULINK environment. The models and optimized simulation code are exported from the MapleSim environment using the Maple CodeGeneration toolbox to MATLAB.

The simulation results of the model following a step-like lane change at the speed of 10 m/s are shown in Fig. 6(*a*). The MPC assigns the steering wheel angle at each time to follow the desired path as closely as possible. Figure 6(*b*) shows the desired steering wheel angle to perform the aforementioned lane change maneuver.

As the driver/steering model has only one degree of freedom, the inverse kinematic simulation result of the vehicle doing a step lane change maneuver provides the angles, angular velocities, and accelerations of all joints. Joint angles at shoulder and elbow are shown in Fig. 7. However, due to the redundancy in the system, the joint torques are not unique for the specified maneuver. With the two optimization criteria mentioned earlier in solving for the joint torques, joint torques and wrist forces have been obtained as shown in Fig. 8. Figures 8(*a*) and 8(*b*) correspond to the wrist reaction force minimization criterion, and Figs. 8(*c*) and 8(*d*) correspond to the joint torque minimization criterion.

It can be observed that the wrist reaction forces found using the first objective function (4) are significantly smaller than those found by minimizing joint torques. Conversely, the calculated joint torques is smaller in the latter case.

The optimal muscle forces can be found from the joint torques with the method presented in Sec. 4. The optimal muscle forces calculated from the torques associated with the wrist force minimization criteria are shown in Figs. 9 and 10. It can be seen that there is little agonist/antagonist cocontraction in muscles force, which indicates that a motion with minimum effort has been performed.

Infraspinatus and trapezius muscles are inactive or insignificantly active, which is consistent with the previous assumption of not considering internal rotation of the shoulder. Deltoid and long head of triceps brachii play the role of the antagonistic muscle in shoulder and elbow, respectively. It can be observed that the deltoid force is smaller than other agonist muscle forces, which can be the result of gravity pulling the arm down and helping to rotate the steering wheel.

When the calculated optimal muscle forces are used in the high-fidelity forward dynamic simulation of the muscle actuated system, the vehicle follows the path shown in Fig. 6(*a*).

Finally, the effect of initial position of hand on the steering wheel is shown in Fig. 11(*b*) while performing a sinusoidal steering task (Fig. 11(*a*)). As expected the initial hand position plays an important role in the computation of joint torques. It can be observed that the grip position has a greater effect on the shoulder torques than elbow torque, and a part of the load is transferred from the vertical rotator of the

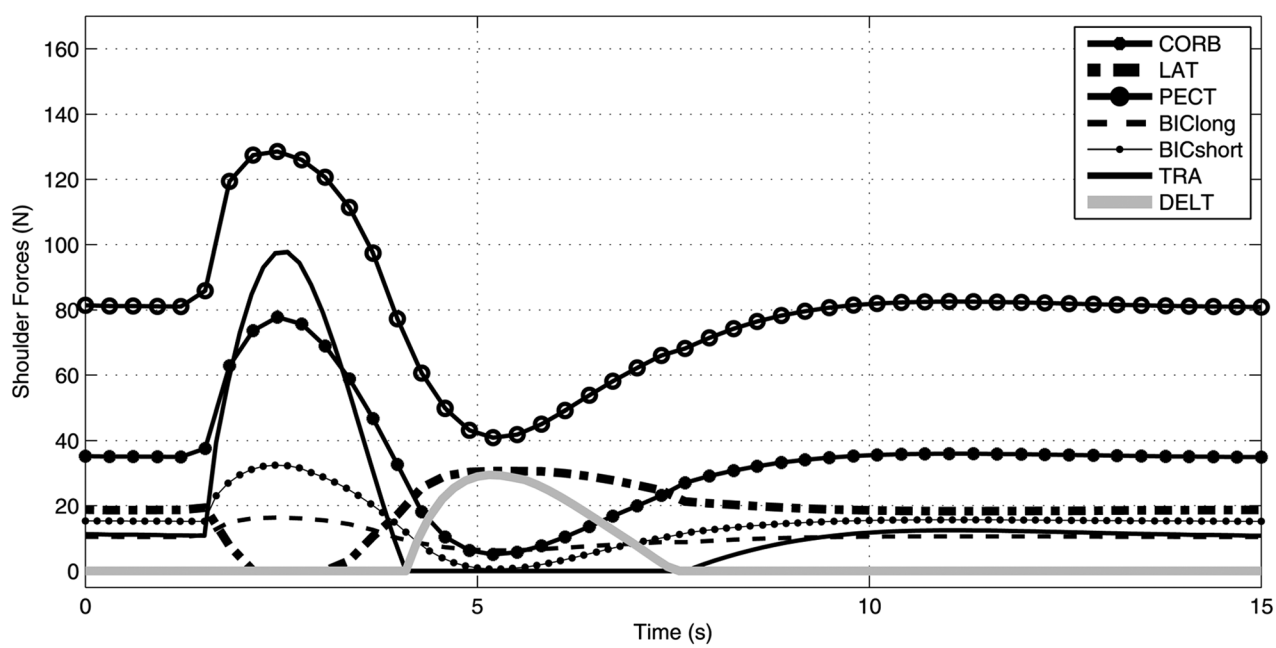

Fig. 10 Optimal muscle forces for the muscles crossing shoulder joint

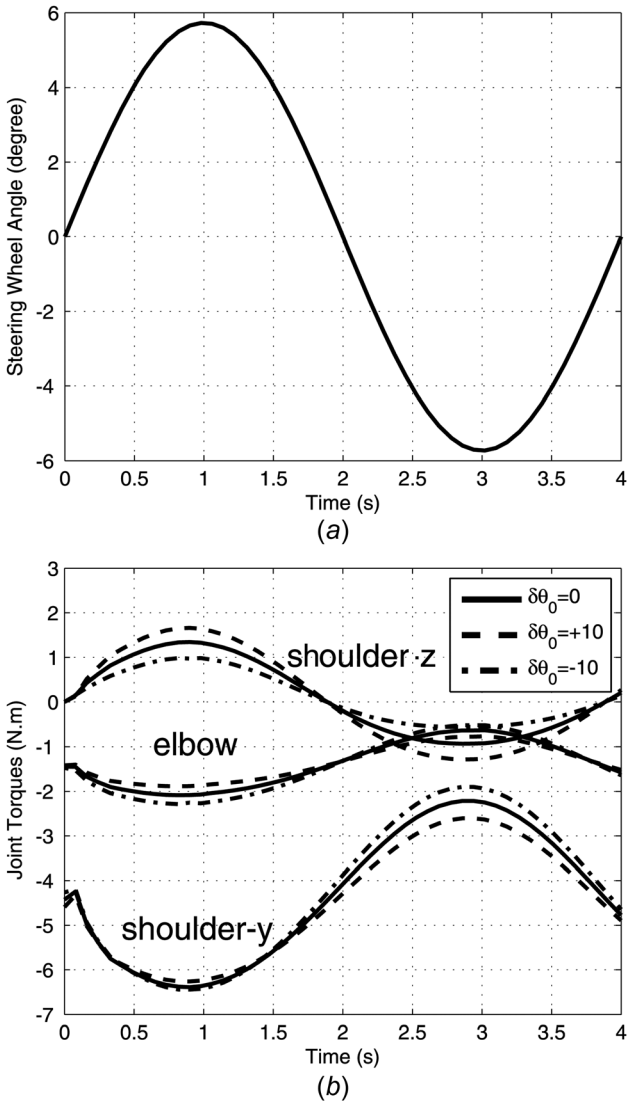

Fig. 11 The effect of changing the steering wheel grip position on the optimal joint torques. (*a*) The steering wheel angle. (*b*) Corresponding joint torque for different grip positions

shoulder to the horizontal rotator by holding the steering wheel on a higher location.

6 Conclusions

Over the past half-century, many research studies have focused on modeling drivers with different degrees of complexity. Much of the research was focused on predicting the steering wheel angle to track a desired vehicle path based on control theories. However, a few research studies included musculoskeletal dynamics of the driver, which contributes to task performance and disturbance rejection.

In this research, a high-fidelity 3D driver's arm model interacting with a detailed vehicle model is used to give in-depth insights into the steering task. Beside the high-fidelity physics-based models, we have also developed a state-of-the-art driver model by employing a hierarchical structure. In this control hierarchy, first, a model predictive controller is used to predict the steering wheel angle for a specific maneuver. Then, a complex controller solves for the optimal joint torques and muscle forces by considering the dynamics of the driver and the vehicle. Finally, a stretch-reflex is added to each muscle to ensure better control precision and disturbance rejection of the motor control.

Using such an architecture enables us to study different aspects of the steering task that could not be investigated otherwise. It is now possible to quantify objective criteria such as decision making (in the MPC), muscle loads, fatigue and cocontraction, as well as the disturbance rejection properties of driver, in a unified simulation. This can facilitate the analysis and design of new assistive steering technologies.

7 Future Work

In this paper, a framework for studying driver/steering interactions was presented. The models, however, were simplified to expedite the work-flow design process. In the future, the validity of the assumptions for kinematics of the arm, including neglected degrees of freedom and muscles, and the effectiveness of the reflex module will be investigated by human testing. Experiments will identify the required modeling enhancements, if any.

As another future objective, Hill muscle models will be added to the driver model. As a result, alternative criteria such as muscle fatigue and metabolic energy consumption can be considered. The effects of such criteria on muscle cocontraction and steering performance will then be studied.

Acknowledgment

The authors would like to thank the Natural Sciences and Engineering Research Council (NSERC) of Canada, Toyota, Maplesoft, and the Ontario Centres of Excellence (OCE) for their support of this research.

Appendix A: Numerical Parameters Values

List of the parameters used in the numerical simulations is presented in Table 3.

Appendix B: Bicycle Model

A linear bicycle model of the vehicle is confined in the path-following controller (MPC) of the driver model. This model can be represented in the following linear state-space representation,

$$\begin{aligned} \dot{\mathbf{x}} &= \mathbf{A}\mathbf{x} + \mathbf{B}u \\ \mathbf{y} &= \mathbf{C}\mathbf{x} \end{aligned} \tag{B1}$$

where x are the state variables and u is the steering wheel angle. The matrices and vectors in Eq. (B1) are written as

Table 3 List of parameters used in the simulations

Parameters	Description	Value	Unit
K_{sw}, C_{sw}	Identified steering stiffness and damping coefficients of the internal model	7.4637, 0.8706	(*N*/rad), (*N*/rad s)
K_p^{sr}, K_d^{sr}	Proportional and derivative coefficients of stretch reflex	6, 1	(mm), (mm/s)
q, r	Weighting factors in the MPC cost function	5, 1	(—),(—)
w_1, w_2	Weighting factors in the static optimization cost function	10, 1	(—),(—)

Table 4 List of identified bicycle model parameters used in the MPC

Parameters	Description	Value	Unit
C_f, C_r	Front and rear tire cornering stiffness	12,635, 20,385	(N/rad)
U_0	Longitudinal vehicle velocity	10	(m/s)
M	Vehicle mass	1106	(kg)
I_z	Vehicle yaw inertia	1990	(kg m^2)
l_f, l_r	Distance to the front and rear axles from CG	0.709, 1.142	(m)
G_r	Steering gear ratio	10.5	(—)

$$\mathbf{A} = \begin{bmatrix} -\dfrac{2C_f + 2C_r}{M U_0} & -\left(U + \dfrac{2l_f C_f - 2l_r C_r}{M U_0}\right) & 0 & 0 \\ -\dfrac{2l_f C_f - 2l_r C_r}{I_z U} & \dfrac{2l_f^2 C_f - 2l_r^2 C_r}{I_z U} & 0 & 0 \\ 1 & 0 & 0 & U_0 \\ 0 & 1 & 0 & 0 \end{bmatrix}$$

$$\mathbf{B} = \begin{bmatrix} \dfrac{2C_f}{MG_r} \\ \dfrac{2l_f C_f}{I_z G_r} \\ 0 \\ 0 \end{bmatrix} \quad \mathbf{C} = \begin{bmatrix} 0 \\ 0 \\ 1 \\ 0 \end{bmatrix}^T \tag{B2}$$

and $\mathbf{x} = [x_1 \quad x_2 \quad x_3 \quad x_4]^T$, where x_3, x_1 are the vehicle lateral position and velocity and x_4, x_2 are the vehicle yaw angle and rate, respectively. The bicycle model parameters and descriptions are shown in Table 4. The parameters are identified using an optimization procedure comparing the lateral response of the high-fidelity vehicle model with the bicycle model.

References

[1] MacAdam, C., 1981, "Application of an Optimal Preview Control for Simulation of Closed-Loop Automobile Driving," IEEE Trans. Syst., Man Cybern., **11**(6), pp. 393–399.

[2] Jalali, K., Lambert, S., and McPhee, J., 2012, "Development of a Path-Following and a Speed Control Driver Model for an Electric Vehicle," SAE Technical Paper 2012-01-0250.

[3] Sharp, R., and Valtetsiotis, V., 2001, "Optimal Preview Car Steering Control," Selected papers from 20th International Congress of Theoretical and Applied Mechanics, Supplement to Vehicle System Dynamics, Vol. 35, pp. 101–117.

[4] Cole, D., Pick, A., and Odhams, A., 2006, "Predictive and Linear Quadratic Methods for Potential Application to Modeling Driver Steering Control," Veh. Syst. Dyn.: Int. J. Veh. Mech. Mobility, **44**(3), pp. 259–284.

[5] Mehrabi, N., Sharif Razavian, R., and McPhee, J., 2013, "A Three-Dimensional Musculoskeletal Driver Model to Study Steering Tasks," International Design Engineering Technical Conference & Computers and Information in Engineering Conferences, Portland, OR.

[6] Droogendijk, C., 2010, "A New Neuromuscular Driver Model for Steering System Development," Master thesis, Delft University of Technology, Delft, The Netherlands.

[7] Sentouh, C., and Chevrel, P., 2009, "A Human-Centered Approach of Steering Control Modeling," Proceedings of the 21st IAVSD Symposium on Dynamics of Vehicles on Roads and Tracks, Stockholm, Sweden, pp. 1–12.

[8] Katzourakis, D., Droogendijk, C., Abbink, D., Happee, R., and Holweg, E., 2010, "Driver Model With Visual and Neuromuscular Feedback for Objective Assessment of Automotive Steering Systems," International Symposium on Advanced Vehicle Control (AVEC), Loughborough, UK.

[9] Pick, A., and Cole, D., 2008, "A Mathematical Model of Driver Steering Control Including Neuromuscular Dynamics," ASME J. Dyn. Syst., Meas., Control, **130**(3), p. 031004.

[10] Pick, A., and Cole, D., 2003, "Neuromuscular Dynamics and the Vehicle Steering Task," The 18th International Association for Vehicle System Dynamics Symposium, Kanagawa, Japan.

[11] Pick, A., and Cole, D., 2006, "Neuromuscular Dynamics in the Driver-Vehicle System," Veh. Syst. Dyn.: Int. J. Veh. Mech. Mobility, **44**(Sup 1), pp. 624–631.

[12] Cole, D., 2008, "Neuromuscular Dynamics and Steering Feel," Proceedings of SteeringTech, TU Munich, Germany.

[13] Ungoren, A., and Peng, H., 2005, "An Adaptive Lateral Preview Driver Model," Veh. Syst. Dyn.: Int. J. Veh. Mech. Mobility, **43**(4), pp. 245–259.

[14] Mehrabi, N., Sharif, M., and McPhee, J., 2012, "Study of Human Steering Tasks Using a Neuromuscular Driver Model," Advanced Vehicle and Control Conference (AVEC), Seoul, Korea.

[15] Pennestri, E., Stefanelli, R., Valentini, P. P., and Vita, L., 2007, "Virtual Musculo-Skeletal Model for the Biomechanical Analysis of the Upper Limb," J. Biomech., **40**(6), pp. 1350–1361.

[16] Gopura, R. A. R. C., Kiguchi, K., and Horikawa, E., 2010, "A Study on Human Upper-Limb Muscles Activities During Daily Upper-Limb Motions," Int. J. Bioelectromagnetism, **12**(2), pp. 54–61.

[17] Liu, Y., Ji, X., Ryouhei, H., Takahiro, M., and Lou, L., 2012, "Function of Shoulder Muscles of Driver in Vehicle Steering Maneuver," Sci. China Technol. Sci., **55**(12), pp. 3445–3454.

[18] Mizuno, T., Hayama, R., Kawahara, S., Lou, L., Liu, Y., and Ji, X., 2013, "Research on Relationship Between Steering Maneuver and Muscle Activities," JTEKT Eng. J., (1010), pp. 13–18.

[19] Maplesoft, a Division of Waterloo Maple Inc., 2014, "Vehicle Model With Double-Wishbone Front and Trailing-Arm Rear Suspension," http://www.maplesoft.com/products/maplesim/modelgallery/detail.aspx?id=67&L=E

[20] van der Helm, F. C. T., Schouten, A. C., de Vlugt, E., and Brouwn, G. G., 2002, "Identification of Intrinsic and Reflexive Components of Human Arm Dynamics During Postural Control," J. Neurosci. Methods, **119**(1), pp. 1–14.

[21] Ting, L. H., van Antwerp, K. W., Scrivens, J. E., McKay, J. L., Welch, T. D. J., Bingham, J. T., and DeWeerth, S. P., 2009, "Neuromechanical Tuning of Nonlinear Postural Control Dynamics," Chaos Woodbury, NY, 19(2), p. 26111.

[22] Hasan, Z., 1983, "A Model of Spindle Afferent Response to Muscle Stretch," J. Neurophysiol., **49**(4), pp. 989–1006.

[23] Kim, N., and Cole, D. J., 2011, "A Model of Driver Steering Control Incorporating the Driver's Sensing of Steering Torque," Veh. Syst. Dyn., **49**(10), pp. 1575–1596.

[24] Uno, Y., Kawato, M., and Suzuki, R., 1989, "Formation and Control of Optimal Trajectory in Human Multijoint Arm Movement," Biol. Cybern., **101**, pp. 89–101.

[25] Crowninshield, R., and Brand, R., 1981, "The Prediction of Forces in Joint Structures; Distribution of Intersegmental Resultants," Exercise Sport Sci. Rev., **9**(1), pp. 159–181.

[26] Röhrle, H., Scholten, R., and Sigolotto, C., 1984, "Joint Forces in the Human Pelvis-Leg Skeleton During Walking," J. Biomech., **17**(6), pp. 409–424.

[27] Happee, R., 1994, "Inverse Dynamic Optimization Including Muscular Dynamics, a New Simulation Method Applied to Goal Directed Movements," J. Biomech., **27**(1), pp. 953–960.

[28] Crowninshield, R., and Brand, R., 1981, "A Physiologically Based Criterion of Muscle Force Prediction in Locomotion," J. Biomech., **14**(11), pp. 793–801.

[29] Cole, D., 2012, "A Path-Following Driver-Vehicle Model With Neuromuscular Dynamics, Including Measured and Simulated Responses to a Step in Steering Angle Overlay," Veh. Syst. Dyn.: Int. J. Veh. Mech. Mobility, **50**(4), pp. 37–41.